[Seatific Journal](https://commons.yildiz.edu.tr/seatific)

Volume 5 | Issue 2 Article 5

2025

Investigation of Maneuvering Coefficients for the Darpa Suboff Aff1 Model via Computational Fluid Dynamics

Haydar Palavar
Department of Plan Approval, Türk Loydu, Tuzla, İstanbul, Türkiye, hpalavar@turkloydu.org

Recommended Citation

Palavar, Haydar (2025) "Investigation of Maneuvering Coefficients for the Darpa Suboff Aff1 Model via Computational Fluid Dynamics," *Seatific Journal*: Vol. 5: Iss. 2, Article 5.
https://doi.org/10.29187/2792-0771.1045
Available at: https://commons.yildiz.edu.tr/seatific/vol5/iss2/5

RESEARCH ARTICLE

Investigation of Maneuvering Coefficients for the Darpa Suboff Aff1 Model via Computational Fluid Dynamics

Haydar Palavar

Department of Plan Approval, Türk Loydu, Tuzla, İstanbul, Türkiye

ABSTRACT

Due to their military applications, submarines are expected to possess certain operational capabilities. Among these, maneuverability stands out as a critical feature, and the investigation and prediction of this capability in the early design stages is of particular importance. In this context, the present study aims to determine the maneuvering coefficients of the DARPA Suboff form's bare hull model (AFF1) by employing the static drift method. Computational Fluid Dynamics (CFD) simulations were conducted in STAR-CCM+, and the results were validated against experimental data available in the literature. As a result of the hydrodynamic effects investigated under various speeds and drift angles, nondimensional maneuvering coefficients were obtained. The results indicate that, at low speeds, the Y_v' coefficient exhibits a significant variation, whereas the N_v' coefficient does not show a substantial change. This suggests that, in low speed maneuvers, the lateral force component is more dominant than the yaw moment.

The comparison of the study's results with the Roddy (1990) experimental data demonstrated low average deviations approximately 3,5% for the X-direction force (longitudinal force), 9,5% for the Y-direction force (sway force), and 5% for the yaw moment; thus confirming the reliability of the numerical model for this geometry. These findings establish CFD as a reliable and efficient alternative method to experimental testing for the analysis of submarine maneuvering performance.

Keywords: DARPA Suboff, CFD, Maneuvering coefficients, Static drift

How to cite this article: Palavar, H. (2026). Investigation of Maneuvering Coefficients for the Darpa Suboff Aff1 Model via Computational Fluid Dynamics. *Seatific*, *5*(2), 112–126. https://doi.org/10.29187/2792-0771.1045

1. Introduction

Throughout history, geopolitical competition and the pursuit of power have driven the development of advanced technologies. As over 70% of the Earth's surface is covered by oceans, maritime dominance has become a key element in global strategic dynamics. Among the most transformative innovations in naval warfare is the submarine, which has significantly reshaped underwater operations. Today, submarines serve a diverse range of purposes, including military operations, scientific exploration, and even tourism. In the defense sector, they play vital roles such as deterrence, strategic offense, force projection, surveillance, and covert attack missions from beneath the surface to shore based targets.

The critical role of submarines in military operations necessitates a range of performance capabilities, among which maneuverability is essential for maintaining operational effectiveness. To successfully conduct reconnaissance and execute underwater missions, submarines must operate at considerable depths with precise control. Additionally, conventional diesel-electric submarines are periodically

Received 17 September 2025; revised 28 December 2025; accepted 6 January 2026.
Published online 19 January 2026

E-mail address: hpalavar@turkloydu.org (H. Palavar).

https://doi.org/10.29187/2792-0771.1045

required to surface to intake atmospheric oxygen—both for engine combustion and for sustaining on-board life-support systems. Consequently, robust maneuvering performance is vital not only in deep-sea environments but also during near surface operations.

During the preliminary design phase of submarines, several maneuvering-related parameters are evaluated, including course-keeping ability, dynamic stability, turning performance, heading-change capability, and stopping behavior. These characteristics are typically assessed using linear motion equations in the early stages of design. While linear methods provide a first order approximation, more complex scenarios—such as those involving propulsion and control systems—require nonlinear modeling techniques. At this stage, maneuvering performance is analyzed using nonlinear mathematical models incorporating surge, sway, and yaw motions. In advanced phases, model testing and Computational Fluid Dynamics (CFD) simulations are employed to enhance the accuracy of maneuverability predictions (Sukas et al., 2017).

Both manned and unmanned submarines are employed for a variety of applications, including scientific research, search and rescue missions, and the maintenance or repair of underwater structures. During such operations—particularly when maneuvering in close proximity to the seabed—the hydrodynamic forces and moments acting on the hull can vary significantly due to ground effect phenomena (Sabuncu, 1985). Consequently, submarines must perform accurate and responsive maneuvers under rapidly changing flow conditions. To ensure safe and effective operation, maneuverability analyses should be conducted prior to the construction phase. These evaluations can be performed using empirical or semi-empirical formulations, Computational Fluid Dynamics (CFD) methods, and physical model testing (Sukas et al., 2017).

Since submarine design is primarily carried out within the defense sector, access to detailed geometries and performance data is often restricted, limiting academic research in this field. To facilitate broader scientific investigation and ensure repeatability across studies, the development and dissemination of standardized submarine model geometries became essential. In response, various institutions and research centers have undertaken efforts to establish publicly available reference models.

In the 1980s, the Defense Advanced Research Projects Agency (DARPA) initiated the SUBOFF project to support the development of submarine technologies. As part of this initiative, a mathematically defined submarine model—available in both appendage and bare hull configurations—was introduced, with its geometric specifications published (Groves et al., 1989). Huang et al. (1989) and colleagues also documented the experimental setup and instrumentation used to test the DARPA SUBOFF model. The symmetric body DARPA SUBOFF model has since been extensively investigated under various configurations. Resistance tests were conducted in towing tanks, while pressure distributions and wake characteristics were examined in wind tunnel environments. Liu and Huang (1998) further analyzed the effects of geometric variations on wake behavior, static pressure fields, and boundary layer velocity profiles. Their study also provided comprehensive datasets on surface pressure and skin friction measurements. The geometry of the DARPA SUBOFF model used in this study is shown in Fig. 1.

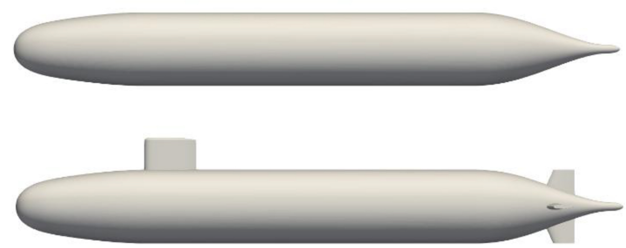

Fig. 1. DARPA suboff model.

Furthermore, the ITTC Manoeuvring Committee (2014) has officially recommended the use of the DARPA SUBOFF models specifically the bare hull (AFF1) and fully appended (AFF8) configurations; as standard geometries for submarine related hydrodynamic studies.

Wu et al. (2005) investigated the influence of hydrodynamic forces acting on submarines operating close to the seabed, with particular emphasis on bottom effect phenomena. In their study, the bottom effect was modeled as a linear function of the vertical distance between the submarine and the seabed. In addition, the influence of the free surface was analyzed for scenarios in which the submarine operated near the water surface.

Vaz et al. (2010) assessed the maneuvering performance of the DARPA SUBOFF model in both appended and bare hull configurations under varying angles of attack. Their study also examined the influence of turbulence models on hydrodynamic predictions by employing two different viscous flow CFD solvers. The findings indicated that distinct configurations of the SUBOFF model are commonly utilized for evaluating the maneuverability of fully submerged bodies. Moreover, the results emphasized that in addition to bottom and free surface effects, frictional forces significantly influence hydrodynamic behavior, and turbulence model selection plays a critical role in simulation accuracy.

Polis et al. (2013) employed Computational Fluid Dynamics (CFD) techniques to examine the maneuvering coefficients of the DARPA SUBOFF model under free surface effects at varying snorkel heights and speeds. In their study, hydrodynamic coefficients accounting for free surface influences were incorporated into a mathematical model developed for submarine simulations. The resulting predictions were found to be in good agreement with experimental measurements.

Duman et al. (2018) investigated the effect of the propeller on maneuvering forces of a submerged body using CFD. Analyses were performed on the DARPA Suboff bare hull form (AFF-1) for different drift angles and Reynolds numbers. Results were validated against experimental data. The study showed that at small drift angles, the propeller significantly affects longitudinal forces but has negligible impact on sway forces and yaw moments. Furthermore, CFD accurately predicts longitudinal forces, sway forces, and yaw moments with high precision.

Atik (2022) investigated the hydrodynamic coefficients of the DARPA SUBOFF submarine using static drift test simulations. CFD results at 0–18° drift angles were validated against experimental data. At small drift angles, the Spalart-Allmaras model showed the closest agreement with experiments, while SST k-ω and k-ϵ models performed better at higher angles. Since all turbulence models produced similar results for sway forces and yaw moments, significant differences in maneuvering behavior are not expected.

Öztürk et al. (2023) numerically investigated the static drift maneuvering forces and moments of the DARPA SUBOFF submarine for AFF-3 and AFF-8 configurations using CFD. The AFF-3 results were validated against experimental data and showed good agreement. For the AFF-8 configuration, where no experimental data were available, the results at 18° drift angle were consistent with the numerical study of Vaz et al. The study showed that with increasing drift angle, the lateral force and yaw moment increase while the axial force decreases, and the presence of the sail significantly affects the maneuvering characteristics.

Çıplakkaya and Arıkan Özden (2023) numerically investigated the forces and moments under static drift and resistance for the model and full scale geometries of the Autosub submarine using CFD. The optimum mesh was determined through a mesh independence study, and results were validated against experimental data. The analysis showed that with increasing drift angle, axial force decreases while lateral force and yaw moment increase.

In addition, Kahramanoğlu (2023) examined the DARPA SUBOFF model in both horizontal and vertical planes under steady speed conditions. In his study on the horizontal plane, he numerically modeled sway and yaw motions at different scales to investigate the scale effects on maneuvering derivatives. Similarly, Kahramanoğlu et al. (2024) conducted a study on the vertical plane, they analyzed heave and pitch motions using CFD and identified the associated scale effects. However, since these investigations were conducted at constant speed, the number of studies addressing results obtained at varying speeds remains quite limited in the literature.

The objective of this study is to determine the maneuvering coefficients of the DARPA SUBOFF form in its bare hull (AFF1) configuration under static drift conditions using CFD. STAR-CCM + software was employed to perform the simulations, and the results were validated against experimental data from the literature. The CFD results were found to be in good agreement with the experiment results, remaining within acceptable accuracy margins. To further ensure result reliability, a grid independence study and uncertainty analysis were conducted. This methodological approach ensured that the findings were not influenced by mesh sensitivity and achieved a balance between computational efficiency and accuracy. The simulations were repeated for multiple speeds, and nondimensional force and moment values were used to derive maneuvering coefficients.

Overall, this study not only provides a validated maneuvering analysis for a widely used submarine geometry but also demonstrates the effectiveness of CFD based methods in capturing hydrodynamic behavior. By comparing the derived coefficients with previous literature, the study contributes to improving the reliability and applicability of computational tools in underwater vehicle design and analysis. Moreover the maneuvering coefficients obtained in this study can be used as reference values in future research and analyses of different DARPA Suboff configurations, thereby providing a new contribution to the existing validated and shareable CFD based maneuvering data in the literature.

2. Methodology

To develop a mathematical model for ship maneuvering behavior, it is essential to define the reference coordinate systems. Two primary coordinate systems are commonly used: the earth-fixed system (o0-x0y0z0) and the body-fixed system (o-xyz). In the earth-fixed system, the origin is typically assigned to the point where the maneuver begins, while in the body-fixed system, the origin is placed at either the ship's midship section or its longitudinal center of gravity (LCG) (Sukas et al., 2017). According to Yasukawa and Yoshimura (2014), positioning the origin at the midship is more appropriate, as the center of gravity may vary with different loading conditions. The earth-fixed and body-fixed coordinate systems adopted in this study are illustrated in Fig. 2.

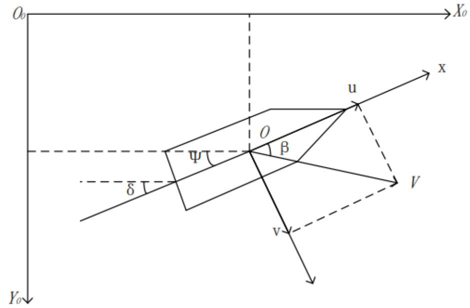

Fig. 2. Fixed (o0-x0y0z0) and slave (o-xyz) axis sets.

In order to model the horizontal plane motion of a ship, it is necessary to determine the linear and nonlinear maneuvering derivatives associated with velocity and acceleration terms. Several approaches are commonly employed to estimate these derivatives (Çakici & Kahramanoğlu, 2017):

- Physical maneuvering experiments (e.g., planar motion mechanism (PMM) tests in yaw and sway, rotating arm tests, and static drift tests)
- Statistical methods such as multiple regression analysis, using data from similar ship models
- Computational Fluid Dynamics (CFD), typically based on the finite volume method

Given the high cost and time requirements of experimental testing, CFD has become a preferred method in both academic and industrial applications. CFD is extensively used for estimating maneuvering derivatives, particularly during the early design stages. Alternatively, regression based approaches using empirical data from comparable hull forms may also be applied.

2.1. Generalized submarine motion equations

The motion of a submarine is described by six degrees of freedom (6DOF), comprising the following components:

1. Surge – Longitudinal translation (x-axis)
2. Sway – Lateral translation (y-axis)
3. Heave – Vertical translation (z-axis)
4. Roll – Rotation about the longitudinal axis
5. Pitch – Rotation about the transverse axis
6. Yaw – Rotation about the vertical axis

The six degrees of freedom motions of a submarine are schematically shown in Fig. 3. Among these, heave, roll, and pitch are primarily governed by hydrostatic restoring forces, while surge, sway, and yaw are considered as the key components of maneuvering motion. In most hydrodynamic studies, submarine maneuvering is modeled using a three degrees of freedom (3DOF) framework that focuses on motion in the horizontal plane.

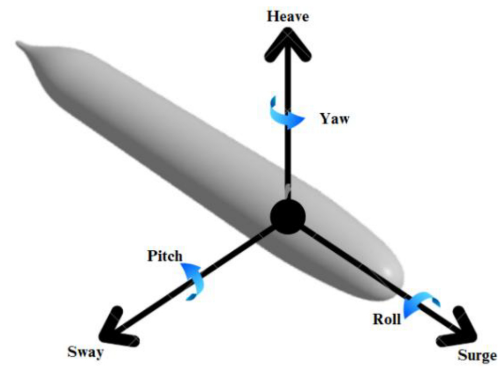

Fig. 3. Submarine motions.

In the earth-fixed coordinate system, external forces and moments acting on the vessel are defined as X_0 in the longitudinal (x) direction, Y_0 in the lateral (y) direction, and N as the yaw moment about the vertical (z) axis. According to Newton's Second Law, the governing equations are expressed as:

$$X_0 = m\ddot{x}_G \tag{1}$$

$$Y_0 = m\ddot{y}_G \tag{2}$$

$$N = I_Z\dot{r} \tag{3}$$

In the equations, $\ddot{x}_G$ represents the acceleration in the x-direction, $\ddot{y}_G$ represents the acceleration in the y-direction, and $\dot{r}_G$ denotes the angular acceleration around the z-axis. Here, x_G and $y_G$represent the coordinates of the ship's center of gravity, while ψ refers to the yaw angle, which is the angle between the ship-fixed coordinate system and the earth-fixed coordinate system. The parameter m denotes the mass of the ship, while I_Z represents the moment of inertia about the z-axis, taken around the center of gravity.

Roddy (1990) conducted comprehensive experiments on submarine motion under six degrees of freedom and published foundational data that remain widely referenced in maneuvering studies. His experimental work, typically analyzed in the earth-fixed coordinate system, has enabled a more detailed understanding of vessel dynamics in multiple directions. Roddy's contributions continue to serve as a critical benchmark for validating numerical and empirical models in submarine maneuvering analysis.

- Surge:

$$m\left[\dot{u} - vr + wq - x_G\left(q^2 + r^2\right) + y_G\left(pq - \dot{r}\right) + z_G\left(pr + \dot{q}\right)\right] = X \tag{4}$$

- Sway:

$$m\left[\dot{v} - wp + ur - y_G\left(p^2 + r^2\right) + z_G\left(qr - \dot{p}\right) + x_G\left(gp + \dot{r}\right)\right] = Y \tag{5}$$

- Heave:

$$m\left[\dot{w} - uq + vp - z_G\left(q^2 + p^2\right) + x_G\left(rp - \dot{q}\right) + y_G\left(rq + \dot{p}\right)\right] = Z \tag{6}$$

- Roll:

$$I_x\dot{p} + (I_z - I_y)qr - (\dot{r} + pq)I_{zx} + (r^2 - q^2)I_{yz} + (pr - \dot{q})I_{xy} + m\left[y_G\left(\dot{w} - uq + vp\right) - z_G\left(\dot{v} - wp + ur\right)\right] = K \tag{7}$$

- Pitch:

$$I_y\dot{q} + (I_x - I_z)rp - (\dot{p} + qr)I_{xy} + (p^2 - r^2)I_{zx} + (qp - \dot{r})I_{yz} + m[z_G(\dot{u} - vr + wq) - x_G(\dot{w} - uq + vp)] = M \tag{8}$$

- Yaw:

$$I_z\dot{r} + (I_y - I_x)pq - (\dot{q} + rp)I_{yz} + (p^2 - r^2)I_{xy} + (rq - \dot{p})I_{zx} + m[x_G(\dot{v} - wp + ur) - y_G(\dot{u} - vr + wq)] = N \tag{9}$$

The parameters in the equations are defined as follows:

m: Mass (submarine displacement + added mass)
I_x: Moment of inertia about the X-axis of the ship
I_y: Moment of inertia about the Y-axis of the ship
I_z: Moment of inertia about the yaw (Z) axis of the ship
u: Surge velocity (longitudinal translation speed)
$\dot{u}$: Surge acceleration (longitudinal translation acceleration)
v: Sway velocity (lateral translation speed)
$\dot{v}$: Sway acceleration (lateral translation acceleration)
w: Heave velocity (vertical translation speed)
$\dot{w}$: Heave acceleration (vertical translation acceleration)
p: Roll angular velocity
q: Pitch angular velocity
r: Yaw angular velocity

3. Darpa suboff numerical analyses

In this study, the determination of maneuvering coefficients for the bare hull (AFF1) model of the DARPA Suboff form in a static drift condition using the CFD method is aimed. The study was conducted using Star CCM+ software, and experimental data from the literature were utilized as a reference to assess the accuracy of the results. The analysis results indicate that the obtained data exhibit consistency with the reference experimental results and fall within acceptable accuracy limits.

3.1. Darpa suboff geometry

The ITTC Manoeuvring Committee (2008) recommended the use of the AFF1 (bare hull) and AFF8 (fully appended) configurations of the DARPA SUBOFF model in submarine hydrodynamic studies. In the present study, the AFF1 geometry was adopted. The model's geometry was sourced from publicly available open access data. Fig. 4 shows the side profile of the form, while Fig. 5 illustrates a perspective view. The main geometric particulars of the DARPA SUBOFF AFF1 model are summarized in Table 1.

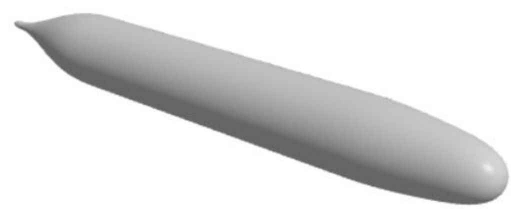

Fig. 4. The perspective view of the DARPA Suboff AFF1 form.

Fig. 5. The side view of the DARPA Suboff AFF1 form.

Table 1. Main dimension.

Length Over All	LOA	4,356 m
Length Between Perpendicular	LBP	4,261 m
Maximum Diameter	Rmax	0,508 m
Longitudinal Center of Buoyancy (fore)	LCB	2,000 m

3.2. Computational domain

The computational domain is of great importance for the analysis. If a smaller than required domain is selected, convergence issues may arise, whereas an excessively large domain increases the number of grid cells, leading to longer solution times. The computational domain was designed as a rectangular prism. To ensure grid resolution accuracy, blocking techniques were applied. The dimensions of the computational domain used in the CFD simulations are shown in Fig. 6.

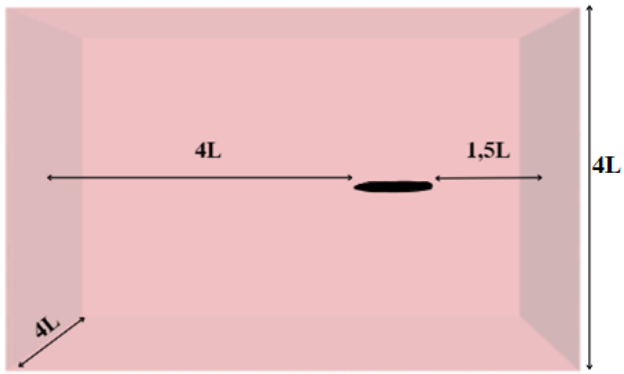

Fig. 6. Computational domain dimensions.

3.3. Mesh structure

The mesh structure is of great importance in CFD analysis. A denser mesh generally increases the accuracy of the analysis. However, an excessive number of mesh elements beyond what is necessary can significantly increase computation time, making the analysis challenging or even infeasible (Demiray, 2020/2021). There are three fundamental mesh structures used for discretizing a CFD solid model: hexagonal, tetragonal, and polyhedral meshes. Among these, the most suitable structure for ensuring high element quality is the hexagonal mesh, which consists of square elements. However, to achieve accurate results for geometries with surface curvature, tetragonal or polyhedral meshes should be preferred over hexagonal meshes.

Other conditions for a high quality mesh structure include the following:

- The transition rate between mesh regions should be minimal.
- In areas with sudden changes, such as the waterline plane and the wake region, the mesh density should be high.
- The skewness ratio in the mesh structure should be kept low.

In this study, block structured domain meshing was applied, and a hexagonal mesh structure was preferred. A prism layer mesh model was also used. The boundary layer is a thin region where fluid viscosity causes interaction between the solid surface and the fluid, playing a crucial role in fluid dynamics analysis. Since this thin layer is a critical region that determines convection and drag forces, accurately modeling it in flow simulations is of great importance. Boundary layer meshes are used to measure properties such as drag force, pressure drop, and flow stability. Such mesh structures enable high resolution modeling in the fluid solid interaction region, enhancing the reliability of the results (Anderson & Wendt, 1995). The boundary layer mesh structure applied in the simulations is presented in Figs. 7 and 8.

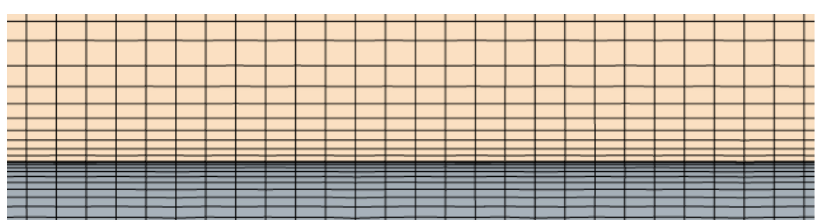

Fig. 7. Boundary layer mesh structure.

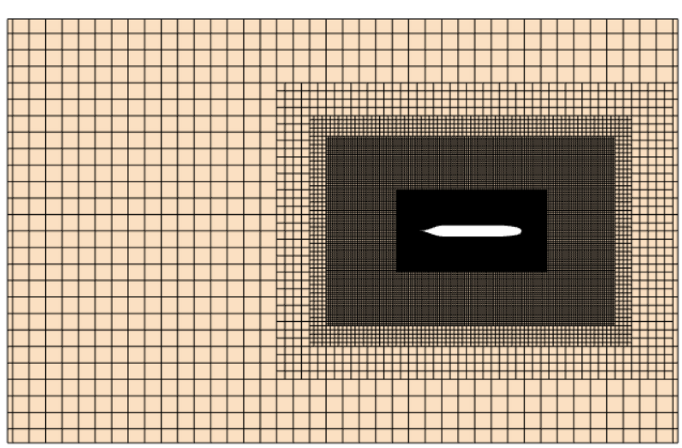

Fig. 8. Mesh structure.

Additionally, it is well known that as the Reynolds number increases, the boundary layer thickness also increases (Cd-Adapco, 2017). This highlights another critical aspect of proper mesh configuration, as higher Reynolds numbers require a more detailed study of complex flow characteristics. The equation for the Reynolds number is:

$$Re = \frac{\rho VL}{\mu} \tag{10}$$

In the given equation, ρ represents the fluid density, V is the velocity, μ is the dynamic viscosity, and L is the characteristic length of the object. In this study, the Reynolds numbers were calculated as $3{,}72 \times 10^6$ at a velocity of 1,029 m/s, $7{,}45 \times 10^6$ at 2,058 m/s, $12{,}1 \times 10^6$ at 3,344 m/s, and $15{,}8 \times 10^6$ at 4,373 m/s. Roddy (1990) reported that the variation of hydrodynamic coefficients with Reynolds number persists up to approximately $10–15\times10^6$, beyond which scale effects become negligible. Therefore, the Reynolds number selected in this study is considered sufficient to represent near full scale hydrodynamic behavior. The boundary layer thickness was determined to be 0,044, with 9 passes and a pass rate of 1,2. In the analyses, The first layer thickness was created to satisfy the condition $30 < y+ < 300$. This selection was made to ensure the proper application of wall functions in the turbulence model and to accurately resolve the boundary layer flow. Appropriate y+ values improve the stability of the numerical solution, optimize computational effort, and enhance the accuracy of the predicted flow. Insufficient or excessively thick first layers can lead to erroneous results in velocity profiles, friction forces, and turbulence parameters.

In this study, the surface remesh method was applied as a secondary step. The surface remesher plays a crucial role in generating high quality mesh structures to enhance solution accuracy in computational fluid dynamics (CFD) analyses and ensure the reliability of the analysis process (Cd-Adapco, 2017). A detailed rearrangement of the surface allows computational models to function more efficiently and enables accurate analysis of parameters influenced by surface properties. Finally, one of the mesh structure models utilized in this study was the Trimmer model. The Trimmer model segments the curved surfaces of geometric structures into functional sections, ensuring that an appropriate mesh structure is generated in these regions (Çavdar, 2022). This method contributes to more precise modeling of wall geometries and provides an effective solution for analyzing particularly complex surface geometries. One of the primary advantages of the Trimmer model is that it simplifies the mesh generation process while improving computational accuracy by adapting to different surface characteristics.

3.4. Boundary conditions

Defining appropriate physical boundary conditions is crucial for ensuring the convergence and stability of a CFD problem. Therefore, it is essential that the boundary conditions are properly defined and compatible with the simulation setup. The boundary conditions used in this study are specified below. Fig. 9 illustrates the applied boundary conditions.

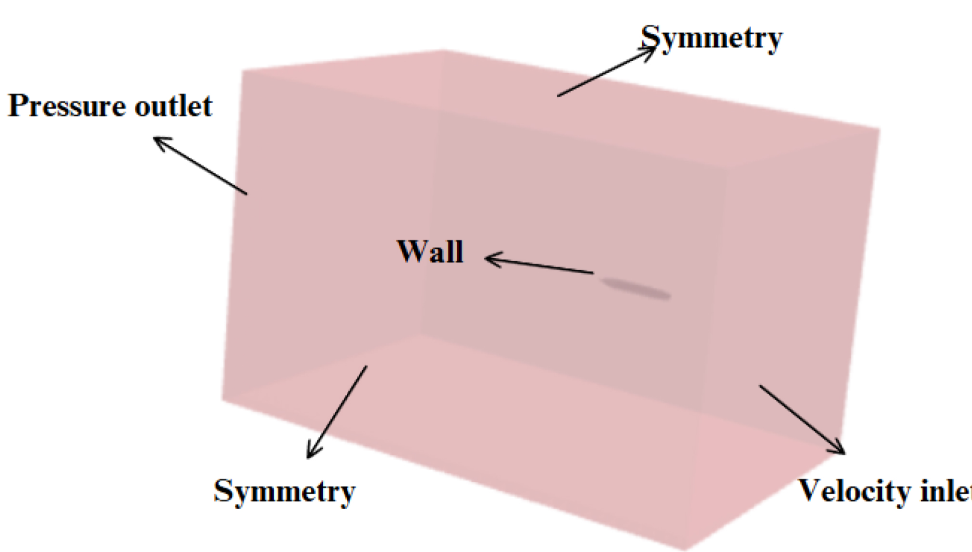

Fig. 9. Boundary conditions.

Velocity Inlet: This boundary condition is used to define the velocity profile in the region where the fluid enters. It determines the flow rate and direction at the inlet.

Pressure Outlet: This boundary condition specifies the pressure values at the region where the flow exits the system. The pressure profile is defined at the outlet to ensure flow equilibrium.

Wall: This boundary condition models the interaction between the solid surface and the fluid. Typically, the no slip condition (zero velocity) is applied, restricting fluid movement along the wall surface.

Symmetry: This boundary condition is used when the flow field exhibits symmetry. It ensures that normal velocity components and other flow parameters remain zero along the symmetry planes, reducing computational effort without compromising accuracy.

3.5. Numerical analysis evaluation

In this section, grid independence studies were conducted alongside the calculation of force and moment values in CFD analyses. The results indicate that the analyses are independent of the grid resolution, and the computed force and moment values are reliable when compared to experimental results. Finally, dimensionless maneuvering coefficients were derived using the force and moment values obtained at various speeds and angles of attack.

3.5.1. Verification analyses

To ensure the accuracy and reliability of the numerical results, grid independence studies were performed. Grid independence analysis is conducted to evaluate the impact of grid density on the accuracy of numerical simulations. In this study, three different grid densities were tested at an 8 degree angle of attack and a speed of 3,344 m/s. The results showed that as grid density increased, the computed force and moment values stabilized after a certain threshold. Beyond this point, further grid refinement did not introduce any significant changes in the results, confirming that the analysis was independent of the grid resolution. A comparison of the forces and moments obtained using different grid densities is presented in Table 2.

Table 2. Comparison of forces and moments for different grid densities.

Grid Density	Grid Number	Grid Size	X(N)	Y(N)	N(Nm)
Course(h3)	675815	1,366	109,33	131,61	789,27
Medium(h2)	1510793	0,975	108,30	130,79	789,89
Fine(h1)	3419121	0,696	107,85	130,35	790,36

The obtained results indicate that the selected grid structure ensures sufficient accuracy for the analysis. Thus, reliable results were achieved while avoiding unnecessary computational costs. For uncertainty analysis, the GCI (Grid Convergence Index) method, based on Richardson extrapolation (RE), was employed. The GCI method is an effective approach to quantify uncertainties related to grid density and to verify whether the simulations are grid independent. In the analysis, the forces in the X and Y directions, as well as the moment (N) around the Z-axis, were examined separately. The steps for calculating the GCI value were as follows:

Grid ratios refer to the ratios between solutions with different grid densities. This ratio is called the grid refinement factor and was calculated as follows:

$$r_{21} = \frac{h_2}{h_1}, r_{32} = \frac{h_3}{h_2} R = \frac{\varepsilon_{21}}{\varepsilon_{32}} \tag{11}$$

Here, r_{21} and r_{32} represent the grid size ratios, while $\varepsilon_{32} = \Phi_3$ - Φ_2 and $\varepsilon_{21} = \Phi_2$ - Φ_1 represent the differences in the number of grid points. R indicates the refinement ratio. After calculating the refinement factors between the dense, medium, and sparse grids, the apparent order of accuracy (p) in the equation can be determined. The approximate p, which represents the solution convergence, is calculated using the following formula:

$$p = \frac{1}{\ln(r_{21})} \left| \ln\left(\frac{\varepsilon_{32}}{\varepsilon_{21}}\right) + q(p) \right| \tag{12}$$

$$q(p) = \ln\left[\frac{r_{21}^p - s}{r_{32}^p - s}\right] \tag{13}$$

$$s = 1.\mathrm{sgn}\left(\frac{\varepsilon_{32}}{\varepsilon_{21}}\right) \tag{14}$$

The following expression was used to calculate the extrapolation value:

$$\Phi_{ext}^{21} = \frac{r_{21}^p \Phi_1 - \Phi_2}{r_{21} - 1} \tag{15}$$

The local relative error and extrapolation error were calculated as follows:

$$e_a^{21} = \left| \frac{\Phi_1 - \Phi_2}{\Phi_1} \right| \tag{16}$$

$$e_{ext}^{21} = \left| \frac{\Phi_{ext}^{12} - \Phi_1}{\Phi_{ext}^{12}} \right| \tag{17}$$

The Grid Convergence Index (GCI) was calculated as follows:

$$GCI_{fine}^{21} = \frac{1,25e_a^{21}}{r_{21}^p - 1} \quad (18)$$

Table 3. The values obtained from the uncertainty calculation are as follows.

	R	r	p	e_a	e_{ext}	%GCI
X	0,43	1,4	2,44	0,00417	0,00327	%0,40
Y	0,52	1,4	1,90	0,00332	0,00372	%0,46
N	0,76	1,4	0,77	0,00059	0,00198	%0,24

When the steps outlined above were applied, the GCI was calculated as follows:

- 0,4084% for the force in the X direction
- 0,4639% for the force in the Y direction
- 0,2488% for the moment (N) around the Z-axis

These low values indicate that the analyses are independent of grid density and provide reliable results. Therefore, the analyses in this study were conducted using a fine grid structure, ensuring both accuracy and efficiency.

3.5.2. Measuring of forces and moments

In this study, analyses were performed using the CFD method at a speed of 3,343 m/s and three different angles of attack. The obtained results were compared with the experimental studies of Roddy and found to be within an acceptable range. The forces in the X and Y directions, as well as the moment around the Z-axis, were examined. The results are shown in Tables 4 to 6. To clearly demonstrate the relative differences between the values, graphs are provided in Figs. 10 to 12.

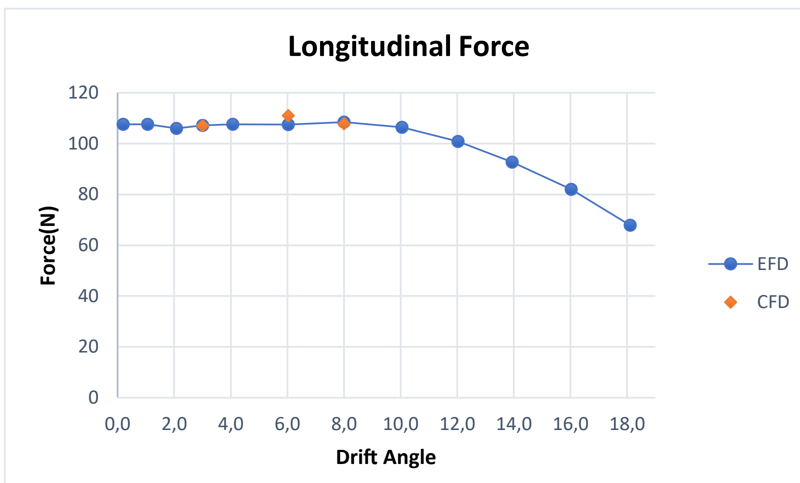

Fig. 10. Comparison of the X-directionforces obtained using the CFD method with experimental results.

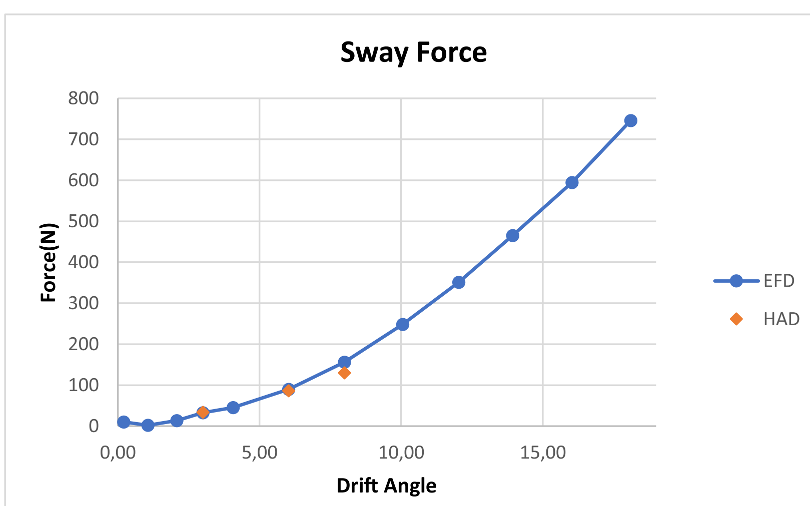

Fig. 11. Comparison of the Y-direction forces obtainedusing the CFD method with experimental results.

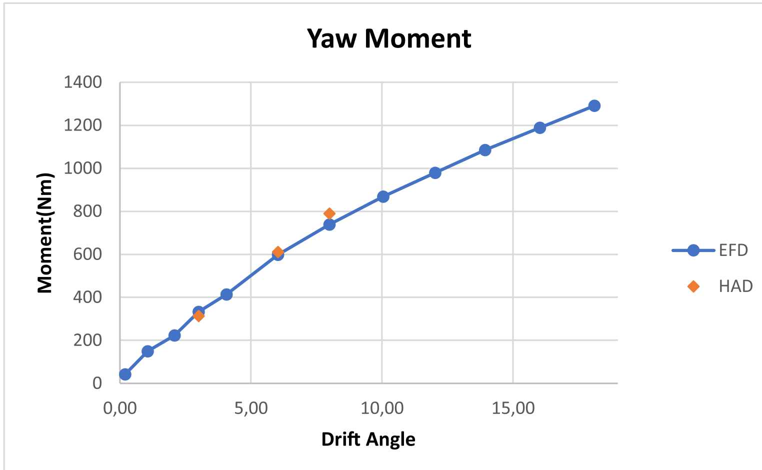

Fig. 12. Comparison of the moment about the Z-axisobtained using the RANS method with experimental results.

Table 4. Comparison of the X-direction forces obtained using the CFD method with experimental results.

Drift Angle	Velocity(m/s)	EFD(N)	CFD(N)	Error (%)
3,00	3,343	111,96	107,05	%4,39
6,03	3,343	112,28	111,04	%1,10
8,00	3,343	113,34	107,85	%4,85

Table 5. Comparison of the Y-direction forces obtained using the CFD method with experimental results.

Drift Angle	Velocity(m/s)	EFD(N)	CFD(N)	Error (%)
3,00	3,343	34,07	34,20	–%0,37
6,03	3,343	93,94	86,37	%8,05
8,00	3,343	162,85	130,36	%19,9

Table 6. Comparison of the moment about the Z-axis obtained using the RANS method with experimental results.

Drift Angle	Velocity(m/s)	EFD(Nm)	CFD(Nm)	Error (%)
3,00	3,343	356,04	313,42	%11,9
6,03	3,343	639,67	611,17	%4,45
8,00	3,343	788,63	790,36	–%0,21

The results obtained from the CFD analysis indicate that the study is reliable when compared to experimental data. Furthermore, it is expected that analyses conducted at higher drift angles may yield significantly different results when compared with experimental measurements. A similar trend was observed by Çıplakkaya and Arıkan Özden (2023) in their study at low speeds ranging from 0.25 to 2 m/s, where good agreement between CFD and experimental results was reported. Examination of the results also shows that as the angle of attack increases, the magnitude of the forces and moments acting on the submarine hull also increases. This behavior can be explained by the rise in lift and drag forces due to changes in the angle at which the flow impacts the hull, leading to higher moment values.

In the second phase of the study, analyses were repeated at different speeds and three different angles of attack. The results are presented in Tables 7 to 9.

Table 7. Force and moment values measured at a 3-degree angle of attack.

Velocity(m/s)	Drift Angle	X(N)	Y(N)	N(Nm)
1,029	3	12,04	3,74	29,15
2,058	3	43,39	13,68	117,93
3,344	3	107,05	34,20	313,42
4,373	3	176,49	56,92	538,13

Table 8. Force and moment values measured at a 6,03-degree angle of attack.

Velocity(m/s)	Drift Angle	X(N)	Y(N)	N(Nm)
1,029	6,03	12,44	9,24	56,93
2,058	6,03	44,80	33,69	230,90
3,344	6,03	111,04	86,37	611,17
4,373	6,03	181,71	139,10	1056,09

Table 9. Force and moment values measured at a 8-degree angle of attack.

Velocity(m/s)	Drift Angle	X(N)	Y(N)	N(Nm)
1,029	8	12,18	14,46	72,82
2,058	8	43,81	52,55	296,28
3,344	8	107,85	130,36	790,36
4,373	8	177,34	216,01	1359,50

As expected, with the increase in speed, the force in the X direction (longitudinal force) increased. This indicates that the submarine's forward resistance increases in direct proportion to speed. Similarly, the increase in the angle of attack caused a significant rise in the forces in the Y direction (sway force) and the moment around the Z-axis (yaw moment). Particularly at high angles of attack and high speeds, the controllability of the submarine may decrease. The primary reason for conducting these analyses at different speeds and angles of attack is to obtain the maneuvering derivatives of the submarine and, through these derivatives, determine the submarine's maneuvering performance.

4. Calculation of maneuvering coefficients

The maneuvering coefficients were obtained using the static drift method. For this, the results from analyses conducted at three different angles of attack and four different speeds were used. The obtained force and moment values were then nondimensional.

Nondimensional is a method used in hydrodynamic analyses and engineering calculations to make physical quantities independent of units. This process facilitates the comparison of systems and conditions at different scales. By eliminating these differences, nondimensional allows data to be interpreted in a more universal manner.

In the study conducted on the DARPA Suboff submarine form, nondimensional allowed the analysis results at different speeds and angles of attack to be examined within a common reference framework.

The nondimensional formula for the force in the X direction is given in Eq. (19), for the force in the Y direction in Eq. (20), for the moment around the Z-axis in Eq. (21), and for speed in Eq. (22).

$$X' = \frac{X}{\frac{1}{2}\rho l^2 U^2} \tag{19}$$

$$Y' = \frac{Y}{\frac{1}{2}\rho l^2 U^2} \tag{20}$$

$$N' = \frac{N}{\frac{1}{2}\rho l^3 U^2} \tag{21}$$

$$v' = \frac{V}{U} = \frac{U sin\beta}{U} = sin\beta \tag{22}$$

He nondimensional X and Y forces, as well as the N moment, calculated using the nondimensional formulas, are presented for different speeds in Tables 10 to 13. To clearly illustrate the differences between the values, the Y'-v' graph in Fig. 13, and the N'-v' graph in Fig. 14.

To calculate the maneuvering derivatives of the Y-direction force (sway) and the moment around the Z-axis (yaw), a linear equation (ax + b) is fitted to the nondimensional values. The least squares method is used for all cases (Yoon et al., 2015). The slope of the Y'-v' graph gives the value of Y_v'. This derivative represents the nondimensional form of the Y_v maneuvering coefficient. Similarly, the slope of the N' - v' graph gives the value of N_v', which represents the nondimensional form of the N_v maneuvering coefficient.

$$Y' = Y_v' v' \tag{23}$$

$$N' = N_v' v' \tag{24}$$

Table 10. Nondimensional X, Y, and N values at a velocity of 1,029 m/s.

Drift Angle	Velocity(m/s)	v'	X(N)	Y(N)	N(Nm)	X'	Y'	N'
3,00	1,029	0,05	12,04	3,74	29,16	0,00120	0,00037	0,00067
6,03	1,029	0,10	12,44	9,25	56,94	0,00124	0,00092	0,00130
8,00	1,029	0,13	12,18	14,46	72,82	0,00121	0,00144	0,00166

Table 11. Nondimensional X, Y, and N values at a velocity of 2,058 m/s.

Drift Angle	Velocity(m/s)	v'	X(N)	Y(N)	N(Nm)	X'	Y'	N'
3,00	2,058	0,05	43,40	13,69	117,93	0,00108	0,00034	0,00067
6,03	2,058	0,10	44,81	33,70	230,90	0,00112	0,00084	0,00132
8,00	2,058	0,13	43,82	52,55	296,28	0,00109	0,00131	0,00169

Table 12. Nondimensional X, Y, and N values at a velocity of 3,344m/s.

Drift Angle	Velocity(m/s)	v'	X(N)	Y(N)	N(Nm)	X'	Y'	N'
3,00	3,344	0,05	107,05	34,20	313,43	0,00101	0,00032	0,00068
6,03	3,344	0,10	111,05	86,38	611,18	0,00105	0,00081	0,00132
8,00	3,344	0,13	107,85	130,36	790,36	0,00102	0,00123	0,00171

Table 13. Non-dimensional X, Y, and N values at a velocity of 4,373 m/s.

Drift Angle	Velocity(m/s)	v'	X(N)	Y(N)	N(Nm)	X'	Y'	N'
3,00	4,373	0,05	176,49	56,93	538,13	0,00097	0,00031	0,00068
6,03	4,373	0,10	181,71	139,20	1056,09	0,00100	0,00077	0,00134
8,00	4,373	0,13	177,35	216,02	1359,50	0,00098	0,00119	0,00172

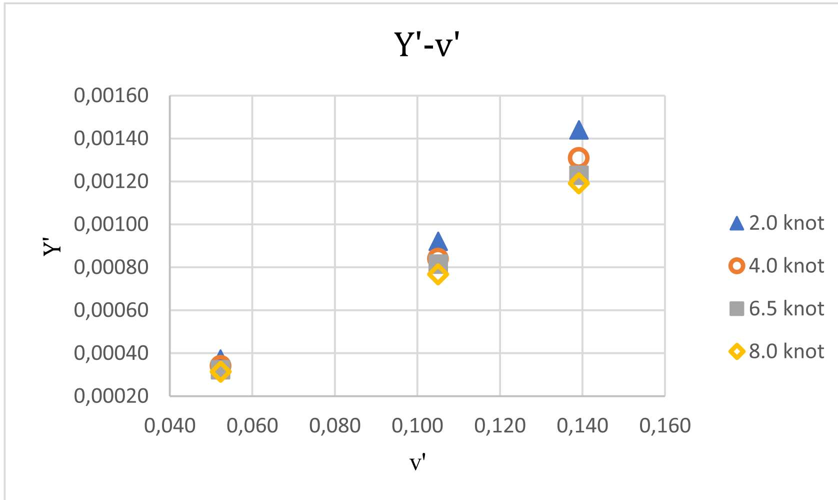

Fig. 13. Y'-v' graph.

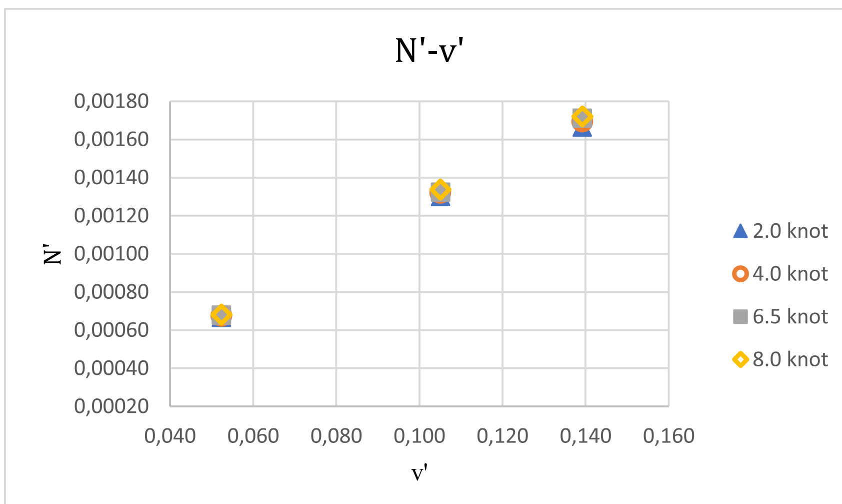

Fig. 14. N'-v' graph.

Table 14. Determination of the nondimensional derivative Y_v' from the Y'–v' graph.

Velocity(m/s)	y=Ax	R^2	$Y_v{}'$	Relative difference with respect to the design velocity of 6.5 kn
1,029	y=0,0096x	0,9885	0,0096	17,1%
2,058	y=0,0087x	0,9888	0,0087	6,1%
3,344	y=0,0082x	0,9907	0,0082	-
4,373	y=0,0079x	0,9895	0,0079	–3,7%

Table 15. Determination of the nondimensional derivative N_v' from the N'–v' graph.

Velocity(m/s)	y=Ax	R^2	N_v'	Relative difference with respect to the design velocity of 6.5 kn
1,029	y=0,0122x	0,9956	0,0122	–2,4%
2,058	y=0,0124x	0,9964	0,0124	-
3,344	y=0,0124x	0,9974	0,0124	-
4,373	y=0,0125x	0,9971	0,0125	1,2%

The reference design speed is 6,5 knots. R^2 represents the accuracy of the fitted curve. R^2 value close to 1 indicates that the curve accurately represents the data. The non-dimensional maneuvering coefficients calculated as a function of velocity are given in Figs. 15 and 16.

When examining the graphs of the obtained nondimensional maneuvering coefficients, the effects of speed changes on the DARPA Suboff submarine form are clearly observed. Specifically, the Y'_v coefficient shows significant variation at low speeds, while the N'_v coefficient is not significantly affected by changes in speed. This suggests that the yaw moment coefficient exhibits a more stable behavior in response to speed variations.

The change in the Y'_v coefficient indicates that lateral forces have a more pronounced effect at low speeds, while the more stable trend of the N'_v coefficient, independent of speed, demonstrates that the forces related to the yaw moment are less influenced by speed.

In the analyses, these coefficients were calculated using the static drift method and CFD techniques, highlighting the effects of speed on the coefficients. These findings provide an important foundation for assessing submarine maneuvering performance and conducting speed based maneuvering analyses.

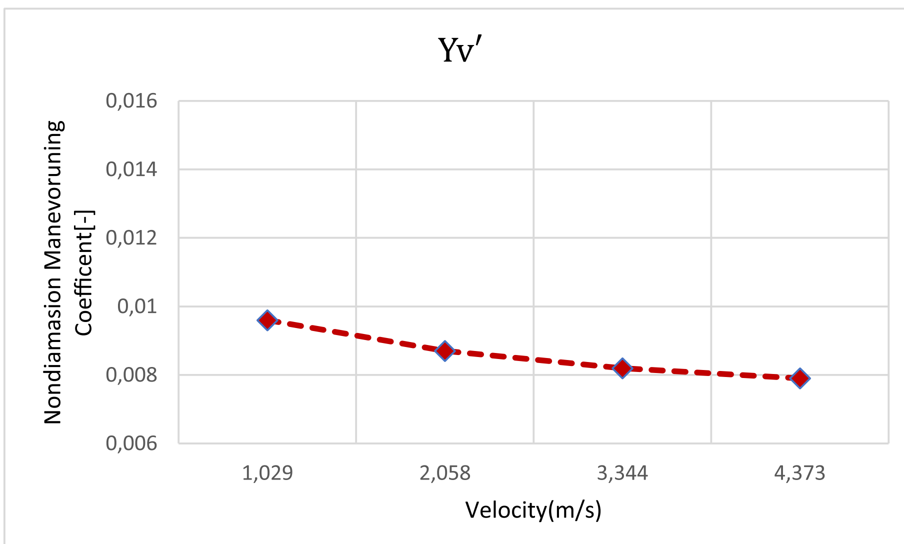

Fig. 15. Non-dimensional maneuvering coefficient.

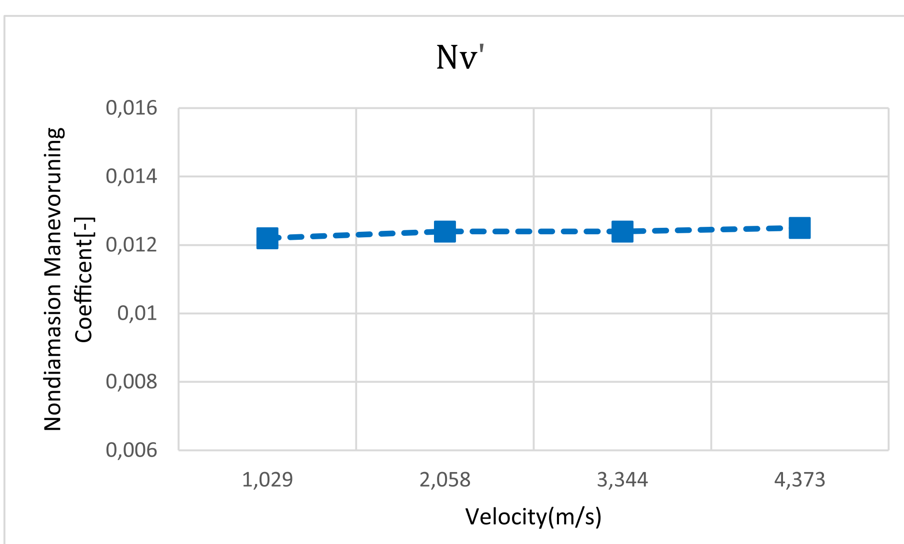

Fig. 16. Non-dimensional maneuvering coefficient.

5. Conclusions

In this study, the hydrodynamic behavior of the DARPA Suboff (AFF1) bare hull under various speeds and angles of attack was investigated using a CFD based static drift method. A mesh independence study was performed at the design speed of 3.343 m/s and an angle of attack of 8 degrees using three different mesh densities, and the optimum mesh structure was identified. The analyses were then repeated for different angles of attack and speeds using the optimum mesh configuration.

To compare the numerical results with experimental data, static drift analyses were conducted at the design speed of 3.343 m/s for angles of attack of 3, 6, and 8 degrees. The forces in the X and Y directions, as well as the moment about the Z-axis, were obtained. When the computed force and moment values were compared with the experimental results reported by Roddy (1990), average deviations of approximately 3.5% for the X-direction force (longitudinal force), 9.5% for the Y-direction force (sway force), and 5% for the yaw moment were observed. These deviation levels are consistent with similar studies in the literature and indicate that the results can provide reliable references for engineering applications. Furthermore, as expected, increasing the angle of attack resulted in a pronounced increase in the magnitude of forces and moments acting on the hull.

To compute the maneuvering coefficients, analyses were repeated at speeds of 1.029, 2.058, 3.344, and 4.373 m/s for angles of attack of 3, 6, and 8 degrees. As expected, the force in the X direction (longitudinal force) increased with speed, indicating that the forward resistance of the submarine rises proportionally with velocity. No significant variation in the X-direction force was observed with changes in angle of attack. In contrast, increases in both speed and angle of attack led to substantial increases in the Y-direction force (sway force) and the moment about the Z-axis (yaw moment). This behavior can be attributed to the expansion of separation zones, the enhancement of pressure asymmetry, and the increasingly irregular distribution of streamlines around the hull at high angles of attack.

The calculated force and moment values were nondimensionalized. To determine the maneuvering derivatives of the Y-direction force (sway) and the moment about the Z-axis (yaw), a linear equation (ax + b) was fitted to the nondimensional values. Examination of the resulting maneuvering coefficients showed that the derivative Y_v' varied significantly within the speed range of 1.029–3.344 m/s, whereas the derivative N_v' exhibited a stable behavior with respect to speed variations. Therefore, it can be stated that the yaw moment coefficient shows a more consistent response to changes in speed.

The validation of the numerical results against experimental data and the successful completion of the mesh independence study demonstrate the reliability of the present work. Additionally, the nondimensional maneuvering coefficients obtained in the study provide reference values for future investigations at different speeds and angles of attack. The maneuvering coefficients and analysis results presented herein are planned to be utilized in future studies involving different experimental configurations (AFF1–AFF8).

Acknowledgments

This paper is derived from the author's undergraduate graduation project conducted at Bandırma Onyedi Eylül University, Department of Naval Architecture and Marine Engineering. The author would like to express sincere gratitude to Assoc. Prof. Dr. Emre Kahramanoğlu for his supervision and guidance, and to Dr. Utku Cem Karabulut for his continuous support and encouragement.

Ethics

There are no ethical issues with the publication of this manuscript.

Conflict of interest

The author declares that there is no conflict of interest.

Financial disclosure

The author declared that this study has received no financial support.

Authors contribution

Conceptualization, methodology, writing, investigation, verification and software: Haydar Palavar.

Data availability statement

The published publication includes all graphics and data collected or developed during the study.

References

Anderson, J. D., & Wendt, J. (1995). *Computational fluid dynamics* (Vol. 206). New York, NY: McGraw- Hill.

Atik, H. (2022). Investigation of turbulence models by using static tow tank tests of DARPA SUBOFF. *Journal of the Faculty of Engineering and Architecture of Gazi University*, *37*(3), 1509–1522.

Cakici, F., & Kahramanoglu, E. (2017). Simulation of turning and zig-zag tests for a fishing vessel hull. (Turkish)

Cd-Adapco, S. (2017). *STAR-CCM+ user guide* (Version 12.04). New York, NY: CD-Adapco.

Çavdar, F. (2022). *Investigation of depth-dependent hydrodynamic maneuvering derivatives and lateral stability in the DARPA submarine model* (Master's thesis, Istanbul Technical University). (Turkish)

Çıplakkaya, S. N., & Arıkan Özden, Y. (2023). Numerical investigation of the resistance and static drift condition of the Autosub submarine. *Seatific*, *3*(2), 71–84.

Demiray, E. (2020, April 4–2021). *ANSYS Fluent – Training Program for CFD Analysis Engineers*. (Turkish)

Duman, S., Sezen, S., & Bal, Ş. (2018). Propeller effects on maneuvering of a submerged body. In *Proceedings of the 3rd International Meeting – Progress in Propeller Cavitation and its Consequences: Experimental and Computational Methods for Predictions* (pp. xx–xx), Istanbul, Turkey.

Groves, N., Huang, T., & Chang, M. (1989). *Geometric characteristics of DARPA SUBOFF models* (DTRC Model Nos. 5470 and 5471). Report No. DTRC/SHD-1298-01.

Huang, T., Liu, H., & Groves, N. (1989). *Experiments of the DARPA SUBOFF program*. David Taylor Research Center, Ship Hydromechanics Department.

ITTC Manoeuvring Committee. (2008). *Final report and recommendations to the 25th ITTC*. Proceedings of the 25th International Towing Tank Conference, Fukuoka, Japan.

ITTC Manoeuvring Committee. (2014). *Final report and recommendations to the 27th ITTC*. Proceedings of the 27th International Towing Tank Conference, Copenhagen, Denmark.

Kahramanoğlu, E. (2023). Numerical investigation of the scale effect on the horizontal maneuvering derivatives of an underwater vehicle. Ocean Engineering, *272*, 113883.

Kahramanoğlu, E., Sezen, S., & Çakıcı, F. (2024). Investigation of scale effects on linear vertical maneuvering derivatives of a submarine. *Journal of ETA Maritime Science*, *12*(1), 14–24.

Liu, H., & Huang, T. T. (1998). *Summary of DARPA SUBOFF experimental program data*. Naval Surface Warfare Center, Carderock Division.

Öztürk, H., Gündüz, K. B., & Arıkan Özden, Y. (2023). Numerical investigation of the maneuvering forces of different DARPA SUBOFF configurations for static drift condition. *Journal of ETA Maritime Science*, *11*(3), 137–147.

Polis, C., Ranmuthugala, D., Duffy, J., & Renilson, M. (2013). Enabling the prediction of manoeuvring characteristics of a submarine operating near the free surface. In *Pacific 2013 International Maritime Conference*, Sydney, Australia.

Roddy, F. R. (1990). *Investigation of the stability and control characteristics of several configurations of the DARPA SUBOFF model (DTRC Model 5470) from captive-model experiments*. David Taylor Research Center.

Sabuncu, T. (1985). *Ship Maneuvering and Control*. Istanbul: ITU Faculty of Naval Architecture and Marine Sciences. (Turkish)

Sukas, Ö. F., Kınacı, Ö. K., & Bal, S. (2017). A General Evaluation for Ship Maneuvering Performance Predictions – Part I. (Turkish)

Vaz, G., Toxopeus, S., & Holmes, S. (2010). Calculation of manoeuvring forces on submarines using two viscous-flow solvers. In *Proceedings of the ASME 29th International Conference on Ocean, Offshore and Arctic Engineering (OMAE2010)*, Shanghai, China.

Wu, B.-S., Xing, F., & Kuang, X.-F. (2005). Investigation of hydrodynamic characteristics of a submarine moving close to the sea bottom with CFD methods. *Journal of Ship Mechanics*, *9*(3), 19–28.

Yasukawa, H., & Yoshimura, Y. (2014). Roll-coupling effect on ship maneuverability. *Ship Technology Research*, *61*(1), 16–32.

Yoon, H., Simonsen, C. D., Benedetti, L., Longo, J., Toda, Y., & Stern, F. (2015). Benchmark CFD validation data for surface combatant 5415 in PMM maneuvers – Part I: Force/moment/motion measurements. Ocean Engineering, *109*, 705–734.